Pergamon

Int. J. Heat Mass Transfer. Vol. 39, No. 5, pp. 1005–1021, 1996

0017–9310/96 $15.00 + 0.00

0017–9310(95)00182–4

Mathematical modeling and experimental measurements of moving boundary problems associated with exothermic heat of mixing

HONGFA HU and STAVROS A. ARGYROPOULOS†

Department of Metallurgy and Materials Science, University of Toronto, Toronto, Ontario, Canada M5S 1A4

(*Received* 2 *November* 1994 *and in final form* 9 *May* 1995)

Abstract—This paper describes a mathematical model which simulates the coupled heat and mass transfer events occurring in moving boundary problems associated with an exothermic heat of mixing. In this class of problems, the heat sink (i.e. latent heat of melting) and heat source (i.e. exothermic heat of mixing) coexist in close proximity. The model was based on the control-volume finite difference approach and on an enthalpy method. The role of heat source acting in this class of problems was simulated by introducing an exothermic heat term into the enthalpy formula.

The computational results indicated that the exothermic heat of mixing leads to a rapid increase of temperature around the moving boundary, which produced an enhanced convective flow in the liquid phase. The intensification of fluid flow around the moving boundary resulted in an acceleration of the melting process. The experimental work reported in this paper was carried out in a low temperature system. In this work, ice cylindrical specimens were immersed in sulfuric acid solutions. The model results were compared with experimental measurements and they were found to be in good agreement.

INTRODUCTION

The modeling of moving boundary problems is an area where mathematicians, engineers of different disciplines and physicists have found a common interest. Although they have divergent perspectives, they all converge in their passion for solving this class of problems. As a result there is an extensive literature addressing the complexity and solution of moving boundary problems. References [1–4] address these problems from different perspectives.

Despite the extensive effort, there is a paucity of information on a class of moving boundary problems when the heat source is very close to the moving boundary. In this class of problems, heat sink (i.e. moving boundary) and heat source (i.e. exothermic reaction) coexist in close proximity, which makes the quantitative analysis of this class of problems very complex. This particular class of moving boundary problems has not only theoretical interest, but has also practical ramifications. A typical case can be found in liquid metals processing operations where exothermic metal additions are melting or dissolving in metal baths [5–12]. In addition, the formation of intermetallic compounds can lead to similar phenomena [13]. So far, the modeling of exothermic metal additions has been carried out by simplifying the problem and looking at it only from the energy contribution of the exothermic reaction [14]. Some physical modeling work on the melting and dissolution of a solid in a liquid with a strong exothermic heat of solution is reported in the literature [15]. In this physical modeling work, ice spheres were immersed in sulfuric acid. Accelerated melting of the ice as well as accelerated fluid flow patterns around the ice sphere were observed. A qualitative explanation was given for the accelerated melting which postulated the existence of a local maximum in the temperature profile. Similar phenomena were observed in independent studies dealing with high temperature systems and they were reported in refs. [8] and [14]. However, so far, this class of problems has not been analyzed quantitatively in any great detail. This is due to the fact that the complex transport phenomena involved are strongly coupled. A rigorous theoretical analysis for this class of problems would require the simultaneous solution of heat, mass and momentum equations.

The objective of this paper is to present a mathematical model which predicts the strongly coupled transport phenomena occurring in moving problems associated with an exothermic heat of mixing. The model is based on an enthalpy method and the SIMPLER algorithm [16]. The model is validated with an experimental investigation which was carried out in a low temperature system. The system chosen for validation is an exothermic one, namely, ice melting in sulfuric acid.

THE PROBLEM AND ITS MATRIX

The moving boundary problems which are associated with an exothermic heat of mixing are charac-

† Author to whom correspondence should be addressed.

NOMENCLATURE

L	length of ice cylinder
v_r, v_z	velocities in r, z directions
r, z	coordinate directions
t	time
p	pressure
g	gravitational acceleration
h	enthalpy
k	thermal conductivity
k_s, k_l, k_{in}	thermal conductivities for solid, liquid and liquid–solid interface
C_A	concentration of sulfuric acid solution
D_A	diffusion coefficient
H_f	latent heat
$\Delta\bar{H}_w$	partial enthalpy of water in sulfuric acid solutions
C_p	heat capacity
C_s, C_l, C_{in}	heat capacities at constant pressure for liquid, solid and liquid–solid interface
T	temperature
T_m	melting temperature
S_1, S_2, S_E	source terms in energy equation.

Greek symbols

ρ	density
μ	viscosity
ν	kinematic viscosity
α_s, α_l, α_{in}	thermal diffusivities for solid, liquid and liquid–solid interface
ρ_{ref}	reference density
ρ_{in}	density for liquid–solid interface
β_T	thermal coefficient of volume expansion
β_C	concentration coefficient of volume expansion
γ	diffusion coefficient in the modified energy equation
Γ_μ, Γ_α, Γ_D	dimensionless diffusion coefficients for the momentum, energy and diffusion equations
λ	liquid fraction.

Superscript

*	dimensionless.

terized by specific physical phenomena. An analysis of these phenomena indicates that the moving boundary problem is further complicated by the presence of a heat source. The reason for this complication is the fact that a heat sink (i.e. melting of a solid) and heat source (i.e. exothermic mixing) occur simultaneously in close proximity. The presence of the heat source in this class of problems has two effects. First, it makes the moving boundary move faster (i.e. melting faster). Second, it enhances the fluid movement in the vicinity of the moving boundary (i.e. accelerated fluid flow conditions). These types of physical phenomena have been observed in molten metals [17, 18] and molten salts [19].

PHYSICAL CONFIGURATION AND MATHEMATICAL FORMULATION

The physical configuration involved the melting of ice cylinders in a container with sulfuric acid. Figure 1 shows a cross section of the experimental system used. In this system the ice was undergoing an inward melting process. Initially the ice was at its melting temperature and the sulfuric acid solution was at room temperature.

In an effort to develop the mathematical formulation for this complex case in the presence of a moving boundary, natural convection, heat source and heat sink, certain simplifying assumptions were made:

(1) the fluid motion of the acid solution is two-dimensional laminar incompressible flow based on the experimental observations;

(2) the thermophysical properties of sulfuric acid solutions are concentration dependent except for density, which varies with both temperature and concentration;

(3) the volume variation associated with phase change and the viscous dissipation are ignored;

(4) the sulfuric acid solution is a Newtonian fluid;

(5) the exothermic heat of mixing exists only in the vicinity of the moving boundary where the local concentrations are less than 90% of bulk value and

(6) the immersion of the ice cylinder into the sulfuric acid is assumed to take place instantaneously.

It should be noted that assumption (5) ensures that the exothermic heat of mixing was accounted for only in the area where the concentration dropped to less than 90% of the bulk value. For example, in the case of 40% sulfuric acid solution, the exothermic heat of mixing is responsible for heat release in an area close to the moving boundary. This area is bounded by the moving boundary on one side (i.e. pure water) to the point at which the concentration of sulfuric acid is 36%. In this case, the amount of heat release varies from 0 to 52822 J kg^{-1}, respectively.

Regression analyses were carried out with the thermophysical data provided in refs. [20, 21]. The resulting relationships describing the variation of

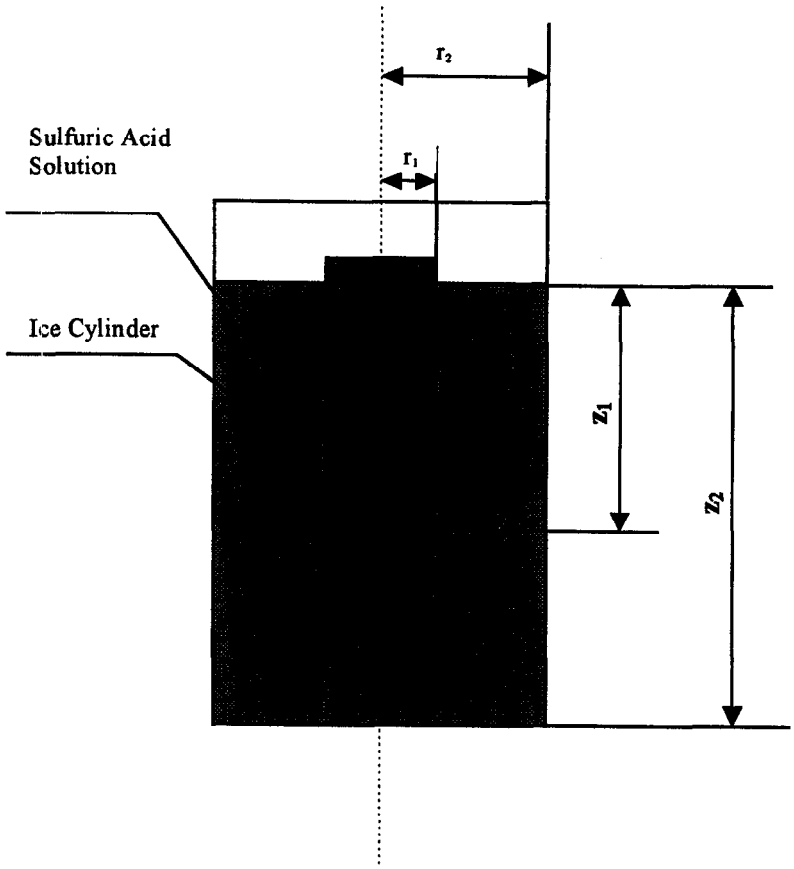

$r_1 = 0.013,\ z_1 = 0.170$

$r_2 = 0.080,\ z_2 = 0.250$

All Dimensions are in Meters.

Fig. 1. Schematic diagram of the system for numerical analysis.

thermophysical properties of solutions are listed in Appendix 1.

The governing differential equations for the laminar and incompressible flow with no viscous dissipation in a cylindrical polar coordinate system can be represented as follows:

Continuity equation:

$$\frac{\partial \rho}{\partial t} + \frac{1}{r}\frac{\partial}{\partial r}(\rho r v_r) + \frac{\partial}{\partial z}(\rho v_z) = 0 \qquad (1)$$

Momentum equation:

r-component:

$$\frac{\partial}{\partial t}(\rho v_r) + v_r\frac{\partial}{\partial r}(\rho v_r) + v_z\frac{\partial}{\partial z}(\rho v_r) = -\frac{\partial p}{\partial r} + \left[\frac{1}{r}\frac{\partial}{\partial r}\left(\mu r\frac{\partial v_r}{\partial r}\right) + \frac{\partial}{\partial z}\left(\mu\frac{\partial v_r}{\partial z}\right)\right] + \left(-\frac{\mu}{r^2}\right)v_r \qquad (2)$$

z-component:

$$\frac{\partial}{\partial t}(\rho v_z) + v_r\frac{\partial}{\partial r}(\rho v_z) + v_z\frac{\partial}{\partial z}(\rho v_z) = -\frac{\partial p}{\partial z} + \left[\frac{1}{r}\frac{\partial}{\partial r}\left(\mu r\frac{\partial v_z}{\partial r}\right) + \frac{\partial}{\partial z}\left(\mu\frac{\partial v_z}{\partial z}\right)\right] + \rho g_z \qquad (3)$$

Energy equation:

$$\frac{\partial}{\partial t}(\rho h) + v_r\frac{\partial}{\partial r}(\rho h) + v_z\frac{\partial}{\partial z}(\rho h) = \left[\frac{1}{r}\frac{\partial}{\partial r}\left(kr\frac{\partial T}{\partial r}\right) + \frac{\partial}{\partial z}\left(k\frac{\partial T}{\partial z}\right)\right] \qquad (4)$$

Diffusion equation:

$$\frac{\partial C_A}{\partial t} + v_r\frac{\partial C_A}{\partial r} + v_z\frac{\partial C_A}{\partial z} = \left[\frac{1}{r}\frac{\partial}{\partial r}\left(D_A r\frac{\partial C_A}{\partial r}\right) + \frac{\partial}{\partial z}\left(D_A\frac{\partial C_A}{\partial z}\right)\right]. \qquad (5)$$

Since the energy equation consists of both convective and diffusive terms in which two dependent variables are included, temperature T and enthalpy h, the Enthalpy Transforming Model [2, 22] is used to convert the energy equation into a non-linear equation with only one dependent variable, enthalpy. Thus, the existing SIMPLER [16] algorithm can easily be implemented. Temperature and enthalpy are related via the following state equation based on thermodynamics

$$\frac{\mathrm{d}h}{\mathrm{d}T} = C(T). \tag{6}$$

If a constant specific heat for each phase is considered, the relation between temperature and enthalpy, when introducing the exothermic heat of mixing ($\Delta \bar{H}_w$), becomes

$$T = \begin{cases} T_m + h/C_s & h \leqslant 0 \\ T_m & 0 < h < H_f. \\ T_m + (h - H_f + \Delta \bar{H}_w)/C_l & h \geqslant H_f \end{cases} \tag{7}$$

The energy equation can be rewritten as follows:

$$\frac{\partial}{\partial t}(\rho h) + v_r \frac{\partial}{\partial r}(\rho h) + v_z \frac{\partial}{\partial z}(\rho h) = \left[\frac{1}{r}\frac{\partial}{\partial r}\left(\gamma r \frac{\partial h}{\partial r}\right) + \frac{\partial}{\partial z}\left(\gamma \frac{\partial h}{\partial z}\right)\right] + S_E \tag{8}$$

where

$$S_E = \left[\frac{1}{r}\frac{\partial}{\partial r}\left(r\frac{\partial S_1}{\partial r}\right) + \frac{\partial^2 S_1}{\partial z^2}\right] + \left[\frac{1}{r}\frac{\partial}{\partial r}\left(r\frac{\partial S_2}{\partial r}\right) + \frac{\partial^2 S_2}{\partial z^2}\right]$$

and where

$$\begin{cases} \text{Solid phase} & h \leqslant 0; & \gamma = k_s/C_s \\ & S_1 = 0 & S_2 = 0 \\ \text{Solid–liquid phase} & 0 < h < H_f; & \gamma = k_{in}/C_{in} \\ & S_1 = 0 & S_2 = 0 \\ \text{Liquid phase} & h \geqslant H_f; & \gamma = k_l/C_l \\ & S_1 = -\dfrac{H_f k_l}{C_l} & S_2 = \dfrac{\Delta \bar{H}_w k_l}{C_l} \end{cases}$$

and where

$$k_{in} = \lambda k_l + (1-\lambda)k_s$$
$$C_{in} = \lambda C_l + (1-\lambda)C_s$$
$$\rho_{in} = \lambda \rho_l + (1-\lambda)\rho_s$$
$$\lambda = \frac{h}{H_f}.$$

As shown, equation (8) is expressed only in terms of a single dependent variable, h, and two source terms of heat sink S_1 and heat source S_2. The transformation of the energy equation simplifies the numerical solution of the present complex case and makes it possible to use the existing algorithm. In order to solve this problem in a more general way, the governing equations should be nondimensionlized. The following dimensionless variables are defined

$$z^* = \frac{z}{L} \quad r^* = \frac{r}{L} \quad v_r^* = \frac{v_r L}{\alpha_l} \quad v_z^* = \frac{v_z L}{\alpha_l}$$
$$h^* = \frac{h}{H_f} \quad \rho^* = \frac{\rho}{\rho_{ref}} \quad t^* = \frac{t\alpha_l}{L^2}$$
$$P^* = \frac{P}{\rho\left(\frac{\alpha_l}{L}\right)^2} \quad S_1^* = \frac{S_1 C_l}{H_f k_l} \quad S_2^* = \frac{S_2 C_l}{H_f k_l}. \tag{9}$$

Since the gravity terms in the momentum equations may have a substantial effect on the fluid flow, the density in the buoyancy forces is dependent on temperature and concentration, based on the assumption that it follows the Boussinesq approximation. Density, temperature, and concentration are related via

$$\rho = \rho_{ref}[1 - \beta_T(T - T_{ref}) + \beta_C(C_A - C_{ref})]. \tag{10}$$

The governing equations can be expressed as the following dimensionless forms by substituting the dimensionless variables from equation (9) into equations (1)–(3), (5) and (8):

Continuity equation:

$$\frac{\partial \rho^*}{\partial t^*} + \frac{1}{r^*}\frac{\partial}{\partial r^*}(r^* v_r^*) + \frac{\partial}{\partial z^*}(v_z^*) = 0 \tag{11}$$

Momentum equation:

r-component:

$$\frac{\partial v_r^*}{\partial t^*} + v_r^*\frac{\partial v_r^*}{\partial r^*} + v_z^*\frac{\partial v_r^*}{\partial z^*} = -\frac{\partial P^*}{\partial r^*} + \left[\frac{1}{r^*}\frac{\partial}{\partial r^*}\left(\Gamma_\mu r^* \frac{\partial v_r^*}{\partial r^*}\right) + \frac{\partial^2 v_r^*}{\partial z^{*2}}\right] + \left(-\frac{\Gamma_\mu}{r^{*2}}\right)v_r^* \tag{12}$$

z-component:

$$\frac{\partial v_z^*}{\partial t^*} + v_r^*\frac{\partial v_z^*}{\partial r^*} + v_z^*\frac{\partial v_z^*}{\partial z^*} = -\frac{\partial P^*}{\partial z^*} + \left[\frac{1}{r^*}\frac{\partial}{\partial r^*}\left(\Gamma_\mu r^* \frac{\partial v_z^*}{\partial r^*}\right) + \frac{\partial^2}{\partial z^*}(\Gamma_\mu v_z^*)\right] - Gr_{mT}(h^* - 1) + Gr_{mC} \tag{13}$$

Energy equation:

$$\frac{\partial h^*}{\partial t^*} + v_r^*\frac{\partial h^*}{\partial r^*} + v_z^*\frac{\partial h^*}{\partial z^*} = \left[\frac{1}{r^*}\frac{\partial}{\partial r^*}\left(r^*\Gamma_\alpha \frac{\partial h^*}{\partial r^*}\right) + \frac{\partial}{\partial z^*}\left(\Gamma_\alpha \frac{\partial h^*}{\partial z^*}\right)\right] + S_E \tag{14}$$

where

$$S_E = \left[\frac{1}{r^*}\frac{\partial}{\partial r^*}\left(r^*\frac{\partial S_1^*}{\partial r^*}\right)+\frac{\partial^2 S_1^*}{\partial z^{*2}}\right] + \left[\frac{1}{r^*}\frac{\partial}{\partial r^*}\left(r^*\frac{\partial S_2^*}{\partial r^*}\right)+\frac{\partial^2 S_2^*}{\partial z^{*2}}\right]$$

Diffusion equation:

$$\frac{\partial C_A^*}{\partial t^*}+v_r^*\frac{\partial C_A^*}{\partial r^*}+v_z^*\frac{\partial C_A^*}{\partial z^*} = \left[\frac{1}{r^*}\frac{\partial}{\partial r^*}\left(\Gamma_D r^*\frac{\partial C_A^*}{\partial r^*}\right)+\frac{\partial}{\partial z^*}\left(\Gamma_D\frac{\partial C_A^*}{\partial z^*}\right)\right] \quad (15)$$

where

$$\begin{cases}\text{Solid phase} & h^* \leqslant 0;\ \Gamma_\mu = \infty\\ \text{Solid–liquid phase} & 0 < h^* < 1;\ \Gamma_\mu = Pr\times 10^{10(1-h)}\\ \text{Liquid phase} & h^* \geqslant 1;\ \Gamma_\mu = Pr\end{cases}$$

$$\Gamma_\alpha = \frac{\alpha_s}{\alpha_l};\quad \Gamma_D = 0;\quad S_1^* = 0;\quad S_2^* = 0$$

$$\Gamma_\alpha = \frac{\alpha_{in}}{\alpha_l};\quad \Gamma_D = 0;\quad S_1^* = 0;\quad S_2^* = 0$$

$$\Gamma_\alpha = 1;\quad \Gamma_D = \frac{Pr}{Sc};\quad S_1^* = -1;\quad S_2^* = \frac{\Delta\bar{H}_w}{H_f}$$

$Pr = \nu_l/\alpha_l$ is the Prandtl number; $Sc = \nu_l/D_A$ is the Schmidt number; $Gr_{mT} = g\beta_T L^3 H_f/\alpha_l^2\rho^* C_l$ is a modified heat transfer Grashof number and $Gr_{mC} = g\beta_C C_A L^3/\rho^*\alpha_l^2$ is a modified mass transfer Grashof number. The initial and boundary conditions are as follows.

Initial conditions

In the domain of calculation, the velocity for the momentum equations is set to zero; the temperature in the ice is set to its melting point; the temperature of the acid solution is specified to be at room temperature (22°C); the concentration is set to the desired value.

Boundary conditions

The radial velocity gradient at the free surface and the vertical velocity gradient on the plane of symmetry are zero. The velocity is set to zero at all solid walls. The temperature and concentration are kept constant at all the solid walls. An adiabatic condition is assumed for the temperature gradient and the concentration gradient at the top surface due to minor changes of temperature and concentration during and after the melting process.

They can be represented in mathematical forms:

Initial conditions

at initial interface between the ice and the solution:

$$v_r = 0,\quad v_z = 0,\quad T = 0°C,\quad C_A = 0,\quad \text{for } t = 0,\quad r = r_1,\quad z = z_1;$$

in the ice:

$$v_r = 0,\quad v_z = 0,\quad T = 0°C,\quad C_A = 0,\quad \text{for } t = 0,\quad 0 < r < r_1,\quad (z_2 - z_1) < z < z_2;$$

in the solution:

$$v_r = 0,\quad v_z = 0,\quad T = 22°C,\quad C_A = \text{constant},\quad \text{for } t = 0,\quad r > r_1,\quad 0 < z < z_2 \quad \text{and } 0 < r < r_1,\quad 0 < z < z_2 - z_1;$$

Boundary conditions

at the axis of symmetry:

$$v_r = 0,\quad \frac{\partial v_z}{\partial r} = 0,\quad \frac{\partial T}{\partial r} = 0,\quad \frac{\partial C_A}{\partial r} = 0,\quad \text{for } r = 0,\quad 0 < z < z_2;$$

at the free surface:

$$\frac{\partial v_r}{\partial z} = 0,\quad v_z = 0,\quad \frac{\partial T}{\partial z} = 0,\quad \frac{\partial C_A}{\partial z} = 0,\quad \text{for } 0 < r < r_2,\quad z = z_2;$$

at the bottom wall and side wall:

$$v_r = 0,\quad v_z = 0,\quad T = 22°C,\quad C_A = \text{constant},\quad \text{for } 0 < r < r_2,\quad z = 0 \quad \text{and } r = r_2,\quad 0 < z < z_2.$$

Tack's technique [23] was adopted for the formulation. The reason for this is that the ratio of the latent heat to the sensible heat is quite high for water–sulfuric acid systems. This causes the large fluctuations in the temperature profiles. Tack's technique was based on an enthalpy balance for the control volume containing the moving boundary combined with linearized temperature profiles near the moving boundary.

The governing equations are discretized with the control volume implicit finite difference procedure referred to as SIMPLER (Semi-Implicit Method for Pressure Linked Equations Revised) [16]. The computational domain actually is half the experimental area shown in Fig. 1 owing to axisymmetry of the current case. The computation is done on a domain with 62×102 nodes. The convergence for each iteration was assured with the dimensionless time step under 8×10^{-7}. The mass source term is within the order of 10^{-5} in the pressure equation, which was used as a criterion of convergence in the fluid flow solution. In addition to this criterion of convergence discussed above, a grid refinement study was performed by doubling the number of nodal points used. In other words, computations were also carried out using a domain with 124×204 nodes. No significant differences were evident between the predictions made using the 124×204 nodes and those made on the basis of the smaller, 62×102 node grid. The predictions for

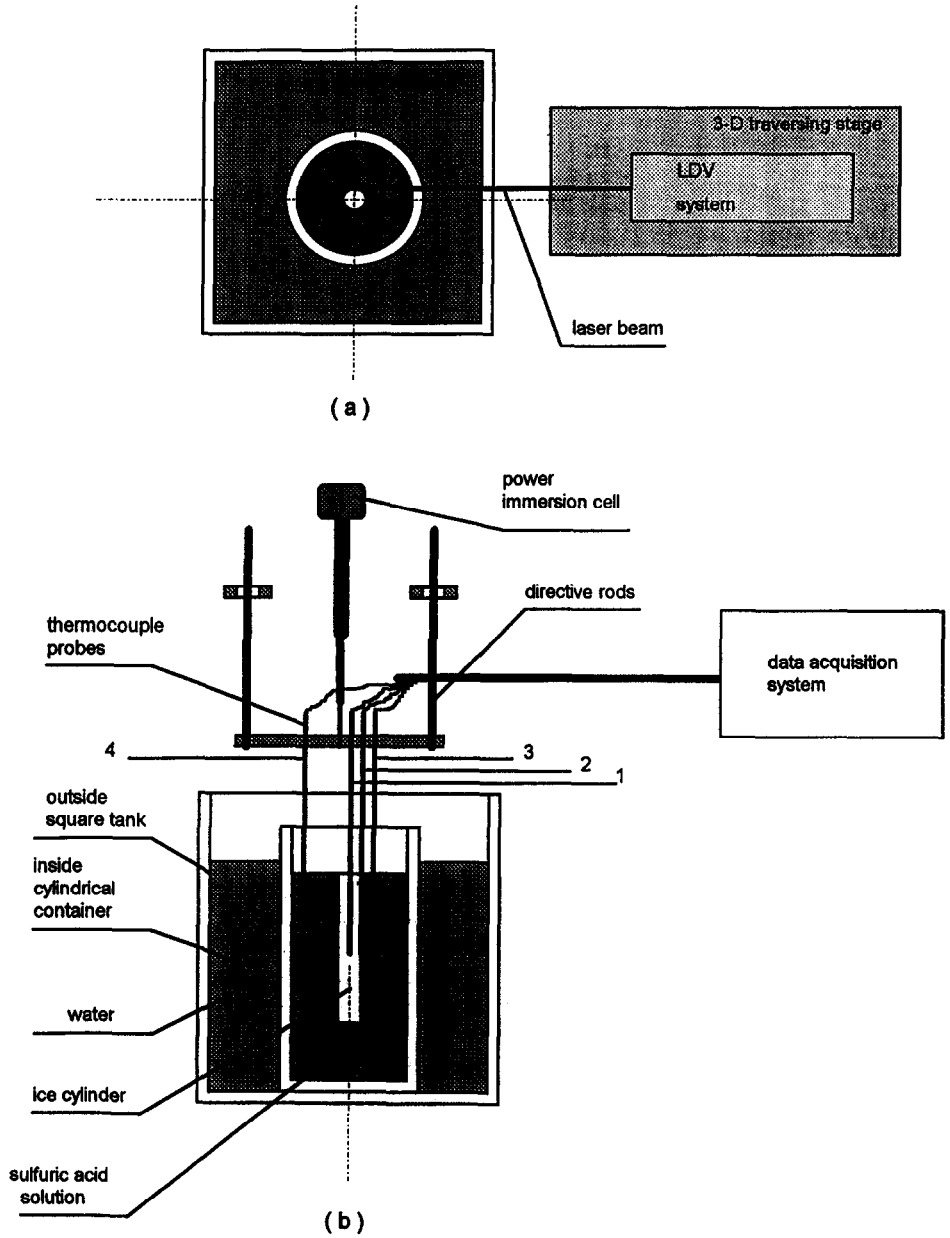

Fig. 2. Schematic diagram of the apparatus: (a) top view; (b) side view.

temperature, velocity, and total melting time did not differ by more than 5% between the two grid sizes.

EXPERIMENTAL APPARATUS AND PROCEDURES

The setup shown in Fig. 2 consisted of a cylindrical container holding the sulfuric acid solution and a square tank in which the cylindrical container sat. The outside square tank was filled with water in order to remove the parallax effect caused by the transverse curvature of the cylindrical container during the experiments. The tank temperature was kept at ambient temperature (22°C).

In the experiment, an ice cylinder with a diameter of 2.54 cm and a length of 17 cm was used. The ice cylinders were made in a copper tube as a mold, 2.54 cm i.d. and 20 cm long. The bottom of the mold was covered with waterproof duct tape to prevent leakage of water. On top of the mold, a hole ($d = 0.16$ cm) in a covering cap was drilled, through which distilled water was injected using a syringe to fill the mold. The distilled water was vigorously boiled to remove dissolved gases. A PFA Teflon (a registered trademark of E. I. DuPont de Nemours & Co.) coated thermocouple probe, serving as a holder for the ice cylinder, was inserted through the hole in the cap concealing the top of the mold to about its center. Then, the

prepared mold was placed in a plexiglass cylindrical container with a few tiny holes at the bottom and then insulated on the top and sides. The tiny holes at the bottom of the plexiglass container ensured that the water froze from the bottom upwards. Any dissolved gas in the distilled water thereafter would rise upwards to form bubbles at the center and near the top surface of the ice cylinder during the freezing process. The entire mold assembly was kept in a freezer maintained at a temperature of $-3°C$ for at least 12 h. When the freezing of the ice was completed, the mold assembly was moved out of the freezer and warmed very slowly to avoid any crack formation on the surface of the ice. The ice cylinder then was removed from the mold and mounted immediately at the position for testing.

Local instantaneous temperatures at a horizontal level about 8 cm beneath the top surface of the acid solution were measured by four specially designed PFA Teflon coated type-K thermocouple probes with a diameter of 0.16 cm. In Fig. 2(b), thermocouple 1 was embedded in the center of the ice cylinder and was used as cylinder holder. Thermocouple 2 was placed in the fluid at a slight distance away from the side of the cylinder. The remaining thermocouples 3 and 4 were positioned 2 and 4 cm, respectively, away from the initial position of the ice cylinder interface. A microprocessor-based data acquisition system, which consisted of a μMAC-6000, a terminal (VC6150) and a host computer (Macintosh SE), was used to record the temperature readings at regular intervals of 500 ms throughout the entire measurement period. It should be noted that the a.d. converter in the μMAC-6000 has 14-bit resolution.

The vertical component of velocities at the initial position of the moving interface was measured at three different horizontal levels about 3, 8 and 12 cm below the top surface of the acid solution, named as levels "III", "II" and "I", respectively. The measurements were made with a TSI dual beam laser Doppler velocimetry (LDV) operating in the back scatter mode. A 15 mW helium-neon laser was used with a beam collimator, a beam splitter and a 480 mm focal length lens to give an ellipsoidal measuring volume with a length of 763.5 μm and a diameter of 82.8 μm. A Bragg cell module was used to shift one of the incident beams so that negative velocities could be measured. Signals originated from the measurement of velocities were sampled with the output of the signal processor going directly to the memory of a microcomputer, IBM 486-DX-50 compatible. TSI's Flow Information Display (FIND) software was used to process the data in order to obtain the velocity plot.

NUMERICAL RESULTS AND DISCUSSION

Typical velocity fields, temperature, and concentration distributions predicted by the computer model in a 40 wt% sulfuric acid solution during the melting process of ice, are illustrated in Fig. 3 through a sequence of vector and contour plots. It can be observed that a marked upward flow in the vicinity of the moving interface between the ice and the bulk solution is predominant in a vertical direction towards the free surface. The flow is deflected as it approaches the vertical solid wall along the free surface. The flow then becomes downstream. After advancing down to one fifth of the depth, the flow tends to move upwards due to the viscous force of the solution. Thus, a recirculating zone is formed at the top part of the container. The eye of the recirculating flow moves towards the left side as the ice melts back. Expectedly, the temperature and concentration distributions caused by the strong convection are similar to the flow pattern. Isotherm and isoconcentration patterns primarily exist around the moving interface and in the top part of the domain. It is evident that the overall velocities of the flow drop as the ice melts away. The recirculating flow spreads mainly in a radial direction and tends to become progressively weaker.

It should be noted that the downward buoyancy force and upward buoyancy force co-exist depending on the temperature and concentration gradients in the vicinity around the moving interface. At the beginning of the melting process, the heat conduction and concentration diffusion are the dominant transport mechanisms. The convection motion starts around the moving interface once the ice melts. Meanwhile, the exothermic reaction also begins in the solution nearby the moving interface due to the mixing of the water with the sulfuric acid solution. The heat released from the reaction results in a rapid increase in temperature around the interface between the ice and bulk solution, which steepens the thermal gradient. Moreover, this increase in temperature also accelerates the melting process, which lessens the concentration gradient and enlarges the concentration boundary layer. As a result, the downward buoyancy force drops abruptly and the upward buoyancy force rises significantly. Thus, the intensified flow is formed that leads to the flow pattern seen in Fig. 3.

Figure 4 shows the velocity fields, temperature and concentration isocontours at four different instants in the melting period of the ice in pure water. In this case, only one downward buoyancy force exists owing to the fact that the density of the fluid at the moving interface is heavier than that in the bulk solution. Flow around the interface is downward instead of upward as the ice melts. Since the flow velocity is very small, a weaker recirculating zone is formed at the bottom of the ice cylinder as a result of the viscous forces. As the melting progresses further, an increasing buoyancy force pushes the recirculating zone downward and towards the bottom, right hand corner of the container. As soon as the ice melts down, the recirculating flow spreads and tends to vanish. It is postulated that the isotherm patterns which appear in Fig. 3 are a consequence of the convection flow.

As seen by comparing the two cases discussed above, the overall velocities in 40 wt% sulfuric acid solutions are almost three times larger than those in

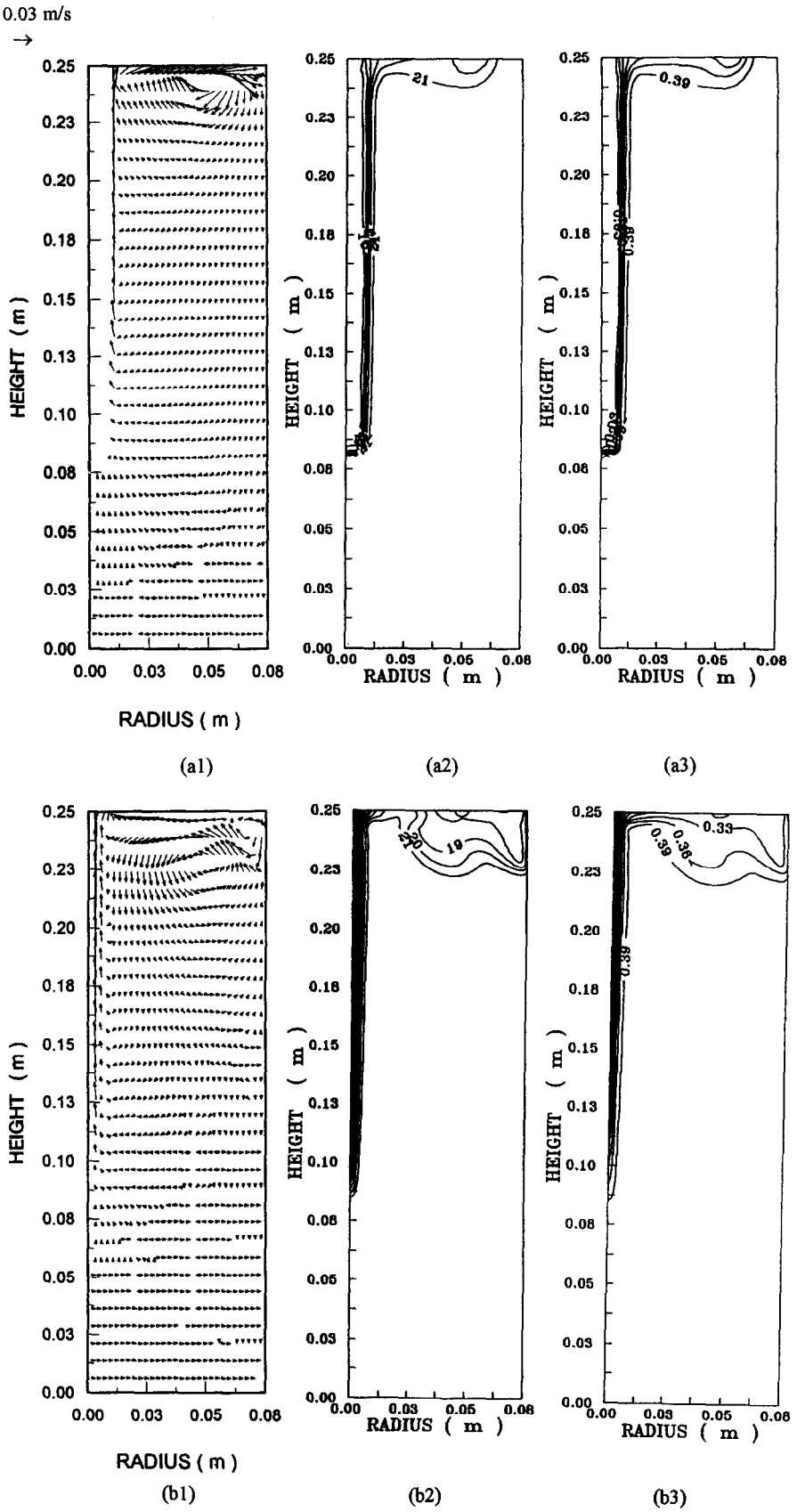

Fig. 3. Ice in 40 wt% sulfuric acid solution at various times after immersion: (a1), (b1) and (c1) velocity fields; (a2), (b2) and (c2) isotherms and (a3), (b3) and (c3) isoconcentrations; at 40, 180 and 380 s, respectively.

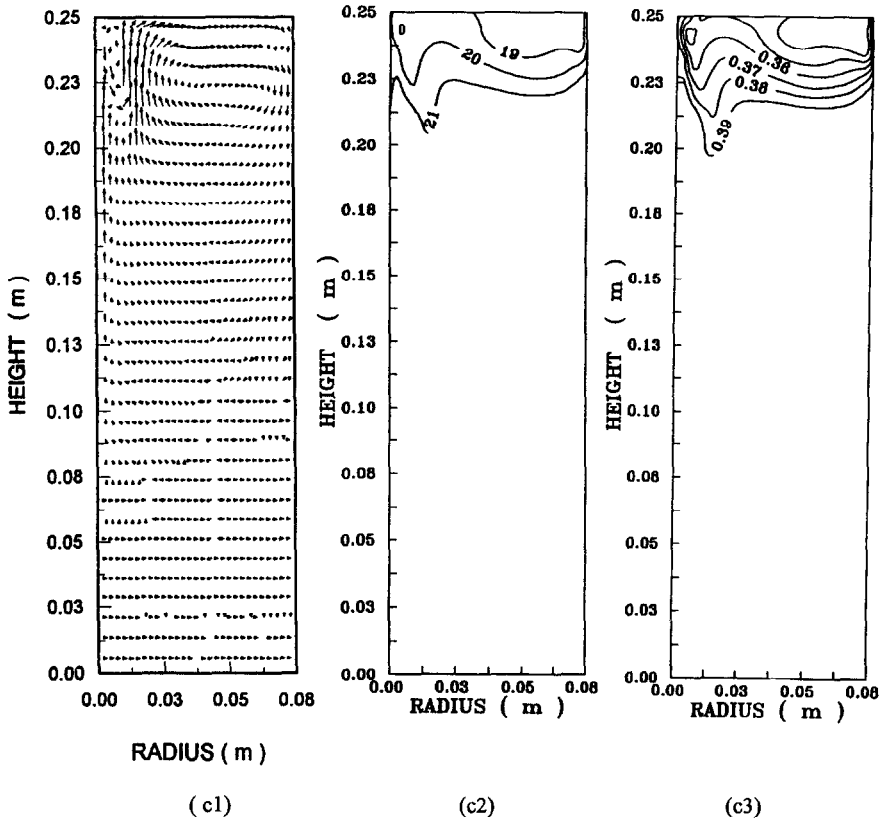

Fig. 3—*continued.*

pure water. It is interesting to note that the thermal stratification is more non-uniform in pure water. This is due to the weaker strength of the flow even two hundred seconds after the ice totally melts away, as can be seen by comparing Figs. 4(d2) with 3(c2). The melting rate in the 40 wt% sulfuric acid solution is more than twice that in pure water. Hence, the exothermic heat, which stimulates the strong convection, definitely plays a key role during and even after the entire melting process.

It is evident from Figs. 3 and 4 that the velocity, temperature and concentration gradients prevail mainly around the moving interface in both concentrations. This implies that characteristics of the boundary layer may dominate the entire melting process in these systems. In order to obtain the detailed picture of the vicinity around the moving interface, a segment of the entire domain was enlarged and is depicted in Figs. 5 and 6. Figures 5 and 6 reveal the area including the ice, boundary layer and a little part of liquid phase near the moving interface. For the 40 wt% solution, because of the higher Schmidt number, $Sc \cong 950$, and higher Prandtl number, $Pr \cong 14.9$, the momentum boundary layer was supposed to be much larger than the thermal and concentration boundary layers. Due to the exothermic reaction and the enhanced flow, however, the cold and pure water supplied from the melting of the ice in a relatively faster way, may enlarge the thermal and concentration boundary layers and keep them at a certain width. Thus, Fig. 5 illustrates that the momentum boundary layer is just sort of larger than both the thermal and concentration layers. In pure water, as anticipated, Fig. 6 shows that the momentum boundary layer is slightly larger than the thermal boundary layer because of the smaller Prandtl number, $Pr \cong 6.9$. By comparing these two cases, it was presumed that the momentum boundary layer in the 40 wt% solution was much larger than that in pure water since the kinematic viscosity of the 40 wt% solution is almost twice that of pure water. But, in the 40 wt% solution, higher velocities of fluid flow might offset the effect of the larger kinematic viscosity on enlarging the momentum boundary layer and reduce the thickness of the momentum boundary layer. Moreover, it may be seen in Figs. 5(b2) and 6(a2) that a steeper thermal gradient exists right beside the moving interface in the thermal boundary layer in the 40 wt% solution as a result of the exothermic reaction taking place, in contrast to the case of pure water, where no exothermic reaction occurs.

COMPARISON OF PREDICTED AND EXPERIMENTAL RESULTS

Experimental work was carried out for the verification of the model predictions. Figures 7 and 8

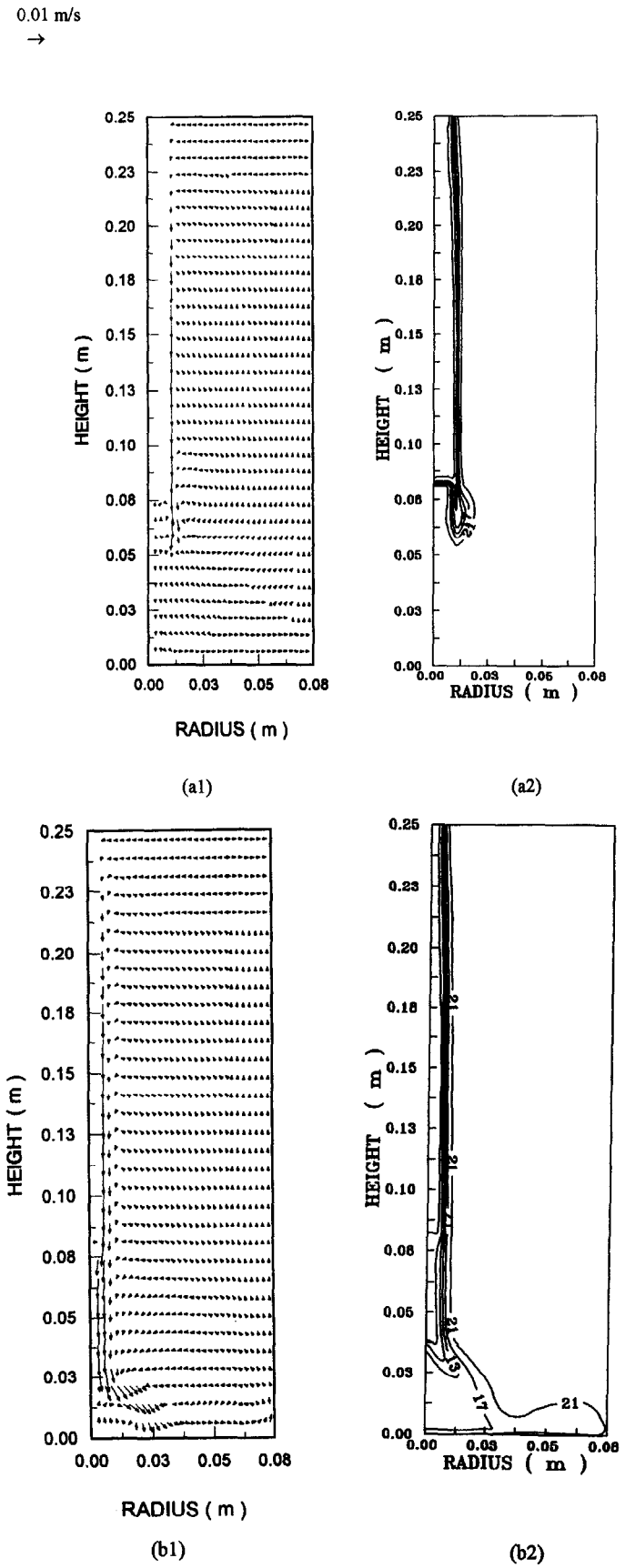

Fig. 4. Ice in pure water at various times after immersion: (a1), (b1), (c1) and (d1) velocity fields; (a2), (b2), (c2) and (d2) isotherms; at 40, 180, 450 and 650 s, respectively.

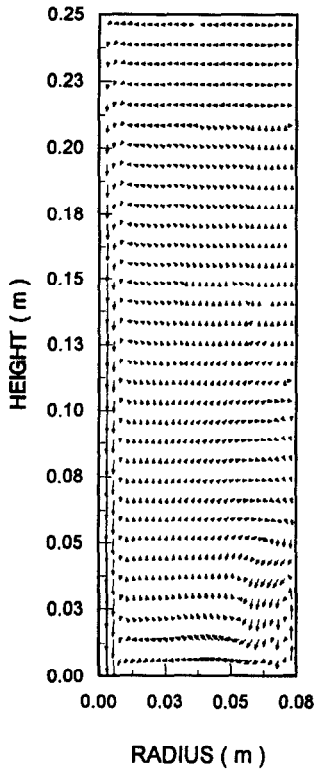

(c1)

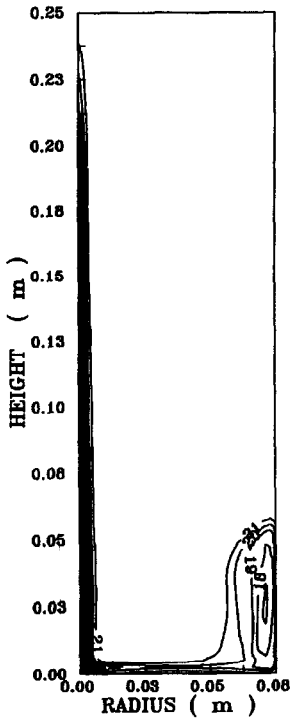

(c2)

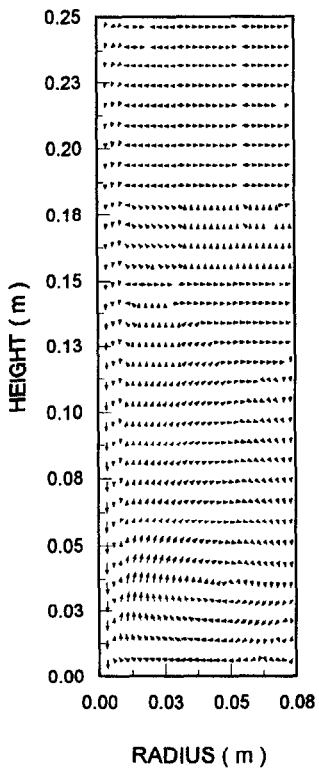

(d1)

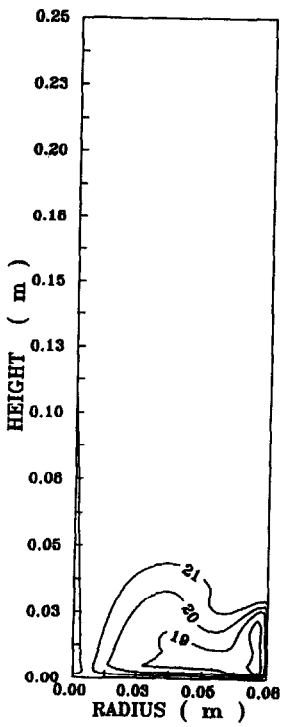

(d2)

Fig. 4—*continued.*

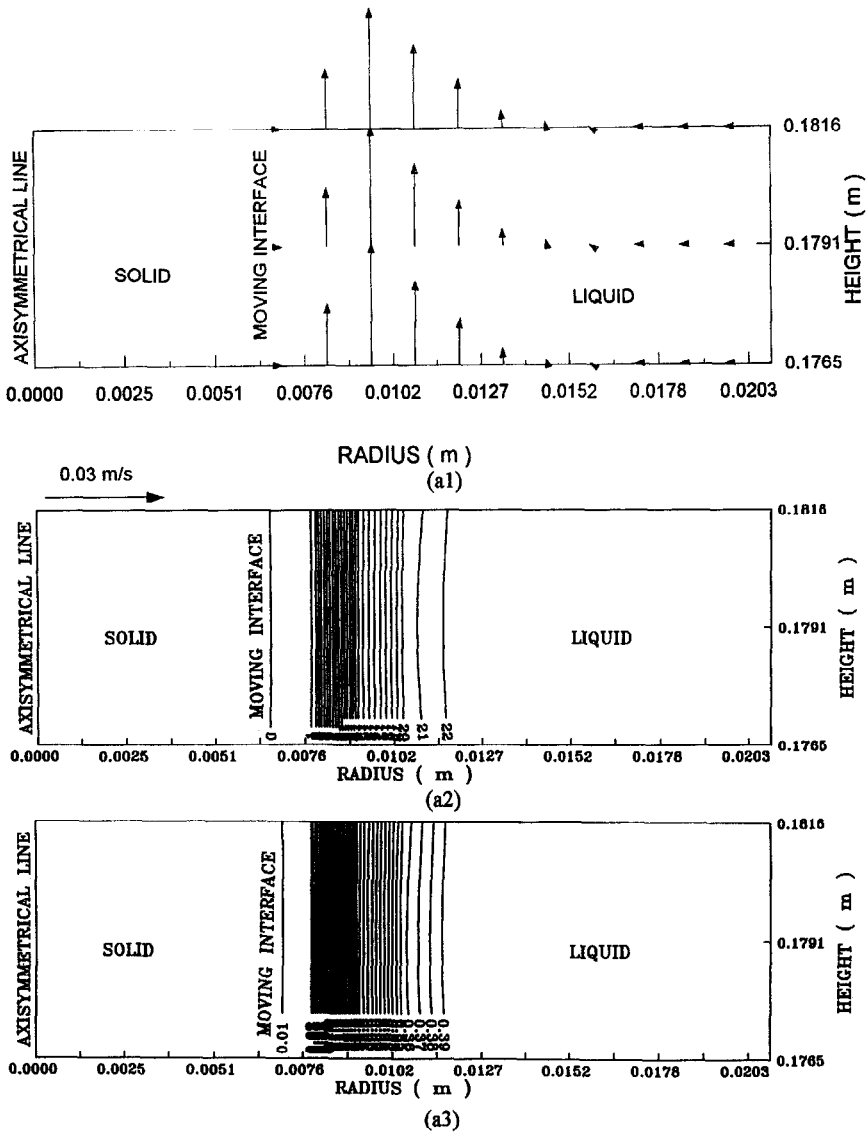

Fig. 5. Enlarged segment around the moving interface at two instants during the melting of the ice in 40 wt% solution: (a1) and (b1) velocity fields; (a2) and (b2) isotherms and (a3) and (b3) isoconcentrations; at 40 and 80 s, respectively.

present the temperature measurements obtained from the experiment. The εMAC-6000 data acquisition system was responsible for measuring the temperature history simultaneously at the four locations in the test section. The temperature at the center of the ice cylinder is represented by line "1", while line "2" characterizes the temperature at the initial position of the moving interface. Lines "3" and "4" give the temperatures at the two different locations far away from the initial position of the interface. The uncertainty associated with the temperature measurements was of the order of ± 0.5°C. The resolution of the a.d. converter in the μMAC-6000 as well as the Teflon protection of the thermocouple tip are two factors contributing to this uncertainty. Figure 7 presents an illustration of the temperature measurement as the ice is immersed into a 40 wt% solution. Segment AB of curve 2 illustrates the period during which the ice cylinder is suspended on top of the sulfuric acid. Segment AB also indicates a temperature which is above the melting point of ice. This is due to the fact that thermocouple 2 is located at a slight distance away from the side of the cylinder. Upon immersion of the ice cylinder at point B, it is worthwhile noting that the temperature at the initial position of the moving interface, which is indicated by segment BC of line 2, increased abruptly from about 3°C to 17°C within a few seconds. The exothermic heat of mixing is responsible for such a phenomenon. After that, the temperature at this position is held around 17°C for about

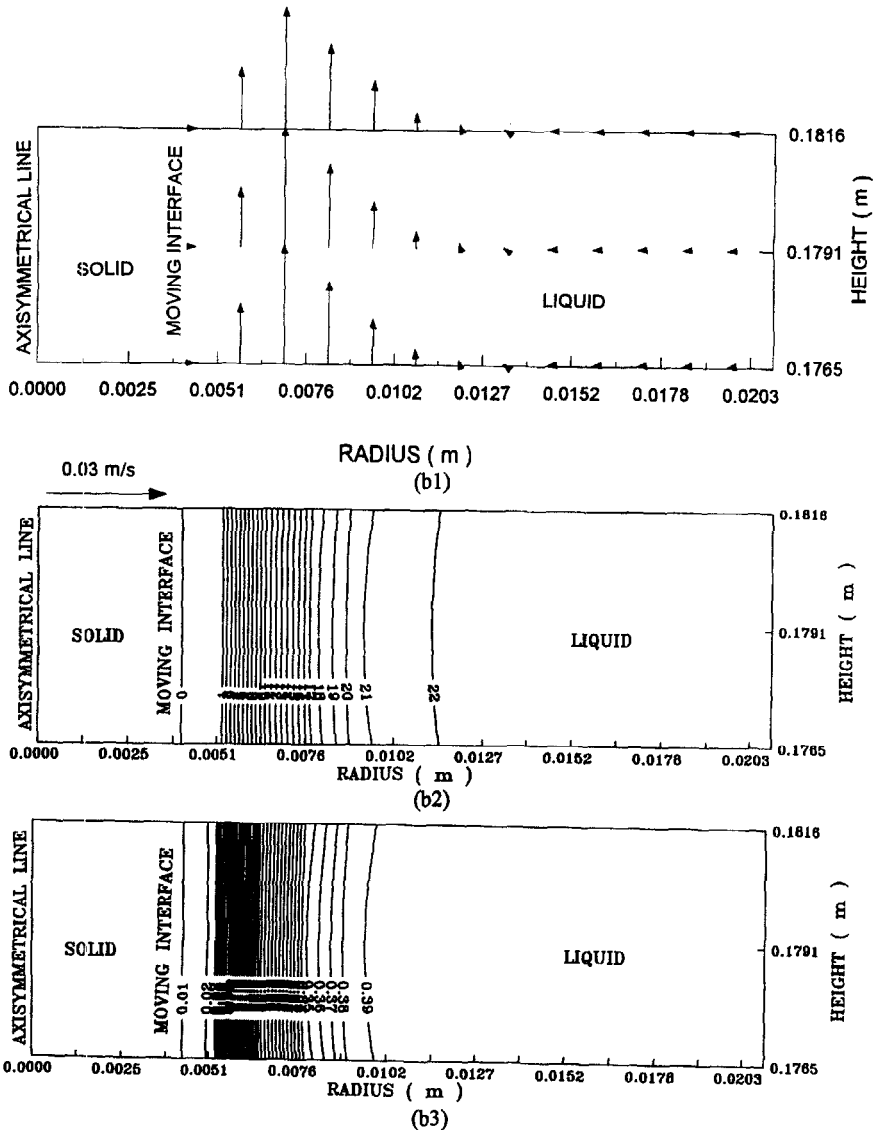

Fig. 5—*continued.*

15 s, represented by segment CD of line 2, due to a large amount of cold water produced from the melting of the ice. Then, the temperature rises again but slowly from point D to point E. Also, the total melting time of the ice, that is, 190 seconds, was recorded by segment FG of line 1. The temperatures indicated by lines 3 and 4 stayed constant at around 22°C during the entire experiment. This observation indicates that a boundary layer effect dominates such a process. Figure 8 shows a typical output from the experiment where the cylindrical ice was melting in pure water. Once the ice was immersed into the solution, the temperature at the initial position of the moving interface, indicated by line 2, started to rise due to the meltback of the ice and the commencement of the convective motion of the fluid. However, compared with the results shown in Fig. 7, it should be noted that the temperature increase was very slow from point B to point C on line 2. It took almost 250 seconds, indicated by segment BC of line 2, compared with a few seconds in the 40 wt% solution. The reason for this slow rise in temperature is that the convection of the solution was too weak, which was caused by small buoyancy forces compared with viscous forces. Segment DE of line 1 depicts the temperature of the ice during the entire melting period. As seen, it remained constant at approximately 0°C. After the ice melted away, it was expected that the temperature registered by segment EF of line 1 increases very quickly because the thermocouple at the center of the ice was exposed directly to the bulk solution. The temperatures indicated by lines 3 and 4 stayed constant at around 22°C during the entire experiment. Segment DE of line 1 marks the total melting time, that is, 470 s. This is

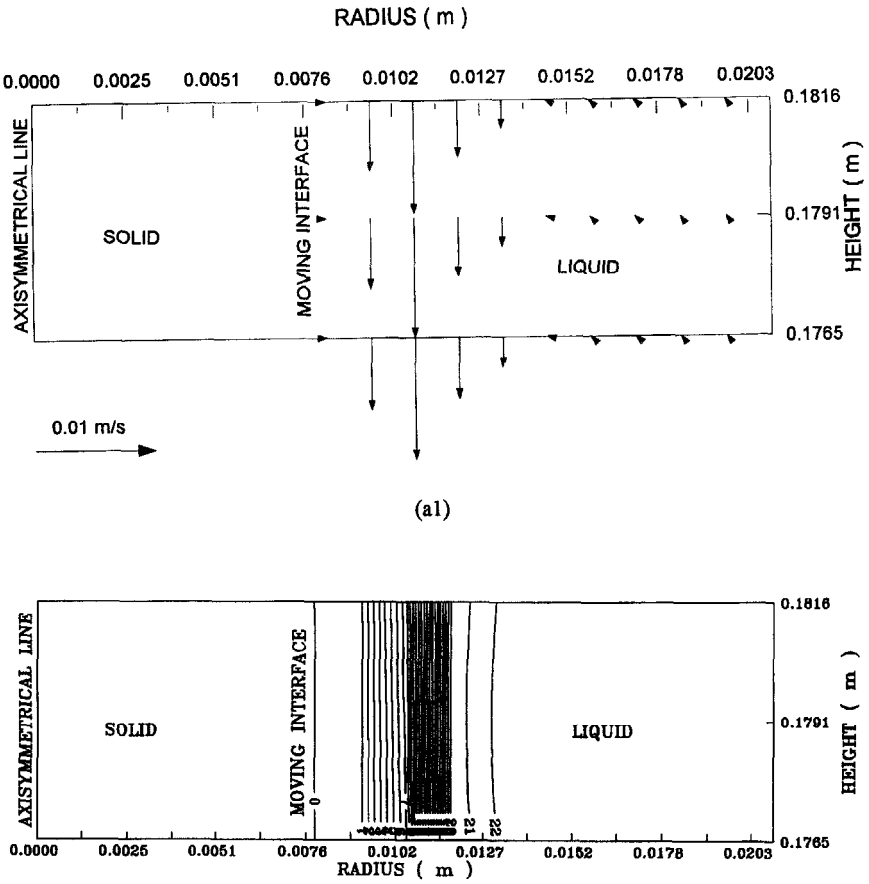

Fig. 6. Enlarged segment around the moving interface at two instants during the melting of the ice in pure water: (a1) and (b1) velocity fields; (a2) and (b2) isotherms; at 80 and 180 s, respectively.

much longer than that of the ice immersion in the 40 wt% solution. The reason for this is that in the 40 wt% solution, the enhanced convection which was activated by the exothermic heat of mixing accelerated the melting process. The remaining features of the temperature illustrated by lines 3 and 4 are similar to those shown in Fig. 7, thus indicating that the melting process in the present case may be controlled by a boundary layer effect as well.

In order to compare the computed and experimental results, the predicted temperature variation of each of the four locations where the experimental measurements were conducted is shown in Figs. 9 and 10 for the 40 wt% solution and pure water, respectively. In general, the predicted and measured temperatures are in close agreement during the entire melting period for both cases. However, the rise of the temperature measured by thermocouple 2 at the beginning of the melting due to the exothermic heat of mixing is slower than that predicted. In addition, the measured plateau CD in Fig. 7 for the 40 wt% solution is longer than the computed one. These discrepancies are, at least in part, due to flow slowdown as a result of the presence of the thermocouple probe, inaccuracy of the thermophysical data used for the computation, and the uncertainty of the temperature measurements.

Figures 11 and 12 show the vertical velocities predicted by the model and those measured experimentally on the three different levels at the 40 wt% solution and pure water, respectively. The results indicate that there is a peak value at all three levels for both solutions, and the vertical velocity in the 40 wt% solution is in the opposite direction to that in pure water. It is important to note that the peak value of the vertical velocity in the 40 wt% solution is almost three time larger than that in pure water. Moreover, the time required to reach the peak value in the 40 wt% solution is about half that of pure water. These results show that the convection of the fluid flow was

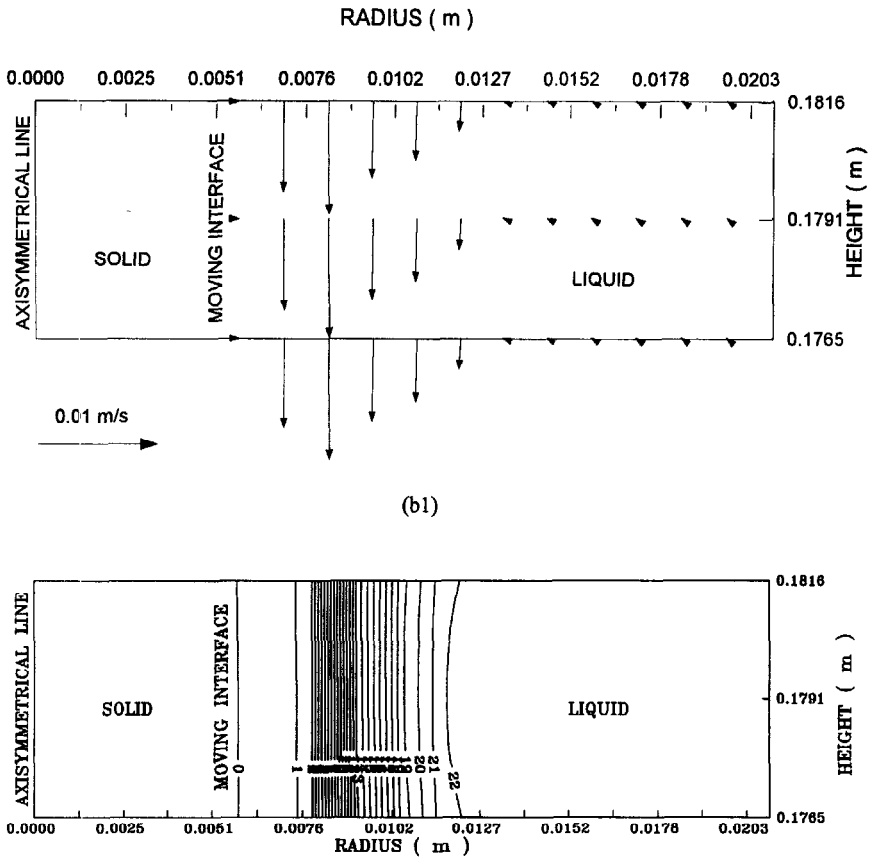

Fig. 6—*continued.*

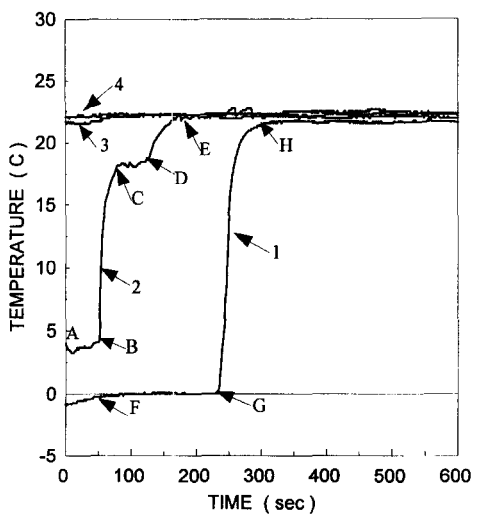

Fig. 7. Typical experimental results of temperature measurements as an ice cylinder melts in 40 wt% solution.

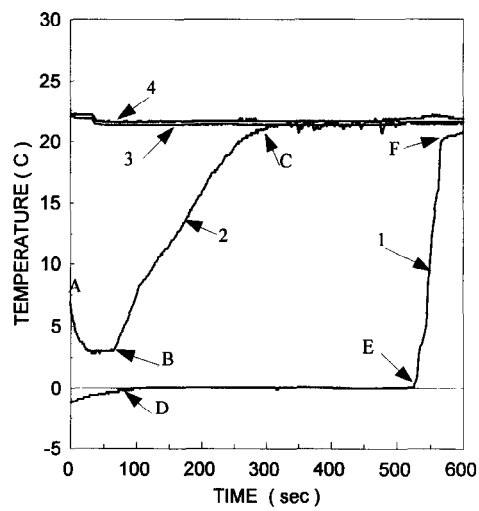

Fig. 8. Typical experimental results of temperature measurements as an ice cylinder melts in pure water.

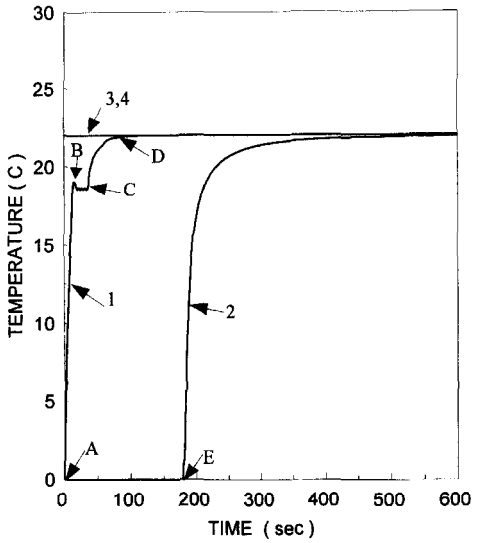

Fig. 9. Computed results of temperature variations as an ice cylinder melts in 40 wt% solution.

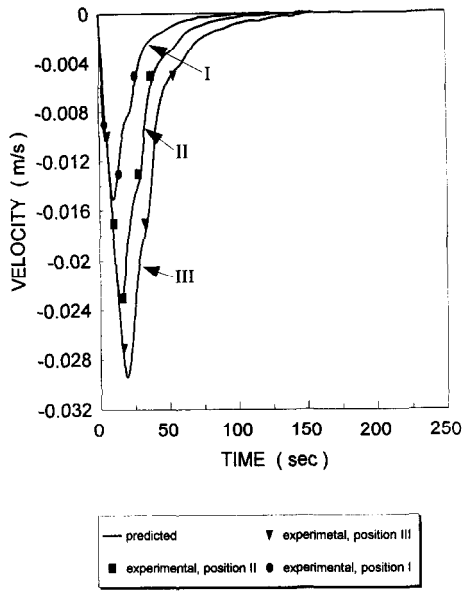

Fig. 11. Comparison of the computed and experimental results of the vertical velocity at the initial positions of the moving interface as an ice cylinder melts in 40 wt% solution.

stronger and the interface between the ice and bulk fluid was moving inwards at a faster rate in the 40 wt% solution than those in pure water. By comparing the predicted output to experimental results, it is seen that they are in good agreement.

CONCLUSIONS

A mathematical model has been developed to simulate the fluid flow, heat and mass transfer phenomena occurring when a moving boundary problem is associated with an exothermic heat of mixing. The results indicate that a strong convection takes place in the presence of the exothermic heat of mixing. This is due to the coupling action between the thermal and concentration fields which results from the exothermic heat of mixing. The melting process is accelerated by the intensified heat transfer and enhanced flow. A boundary layer effect plays a prominent role in such a process. It was also found that the strong recirculating flow improves the mixing conditions during and even immediately after the melting process. The predictions of the mathematical model are found to be in very good agreement with the experimental results. The

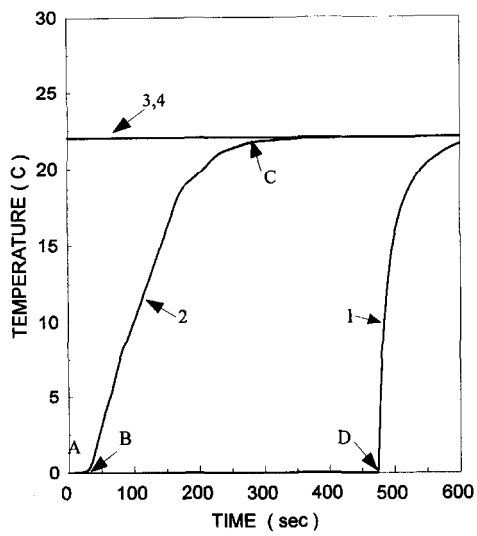

Fig. 10. Computed results of temperature variations as an ice cylinder melts in pure water.

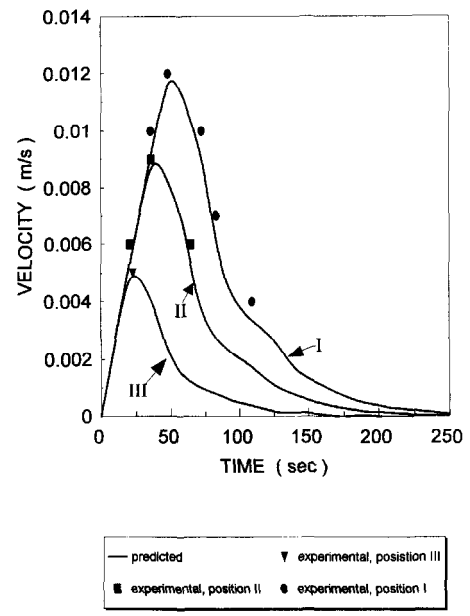

Fig. 12. Comparison of the computed and experimental results of the vertical velocity at the initial positions of the moving interface as an ice cylinder melts in pure water.

results provide some insight as to how the exothermic heat of mixing affects melting processes in general.

Acknowledgements—The authors would like to express their gratitude to the University Research Incentive Fund of the province of Ontario. In addition, they would like to thank the Natural Sciences and Engineering Research Council of Canada for an equipment grant which enabled them to make the Laser Doppler velocimeter operational.

REFERENCES

1. J. Crank, *Free and Moving Boundary Problems*. Oxford Science Publications, New York (1984).
2. V. Alexiades and A. D. Solomon, *Mathematical Modeling of Melting and Freezing Processes*. Hemisphere, Washington (1993).
3. M. Salcudean and Z. Abdullah, On the numerical modeling of heat transfer during solidification processes, *Int. J. Numer. Meth. Engng* **25,** 445–473 (1988).
4. M. Zerroukat and C. R. Chatwin, *Computational Moving Boundary Problems*. John Wiley, New York (1994).
5. S. A. Argyropoulos, On the recovery and solution rate of ferroalloys, *Trans. ISS* (May) pp. 75–86 (1990).
6. S. A. Argyropoulos and R. I. L. Guthrie, The exothermic dissolution of 50 wt% ferro-silicon in molten steel, *Can. Metall. Quart.* **18,** 267–281 (1979).
7. S. A. Argyropoulos, The effect of microexothermicity and macroexthermicity on the dissolution of ferroalloys in liquid steel, *Electric Furnace Proceedings*, Vol. 42, pp. 133–148. ISS-AIME (1985).
8. S. A. Argyropoulos and R. I. L. Guthrie, The dissolution of titanium in liquid steel, *Metall. Trans. B* **15B,** 47–58 (1984).
9. S. A. Argyropoulos and P. G. Sismanis, The mass transfer kinetics of niobium solution into liquid steel, *Metall. Trans. B* **22B,** 417–427 (1991).
10. J. Schade, S. A. Argyropoulos and A. McLean, Core-wire microexothermic alloys for tundish metallurgy, *Electric Furnace Proceedings*, Vol. 46, pp. 17–32. ISS-AIME (1988).
11. J. Schade, S. A. Argyropoulos and A. McLean, Assimilation and recovery characteristics of innovate cored wire additions for steelmaking, *Can. Metall. Quart.* **30,** 213–225 (1991).
12. P. G. Sismanis, S. A. Argyropoulos and P. D. Deeley, The dissolution of microexothermic alloying additions to cast iron, *Electric Furnace Proceedings*, Vol. 43, pp. 39–55. ISS-AIME (1986).
13. G. H. Rodway, J. D. Hunt, The reaction of liquid metals to form intermetallics, *J. Mater. Sci.* **23,** 814–822 (1988).
14. P. G. Sismanis and S. A. Argyropoulos, Modeling of exothermic dissolution, *Can. Metall. Quart.* **27,** 123–133 (1988).
15. J. Szekely and Y. K. Chuang, On the melting and dissolution of a solid in a liquid with a strong exothermic heat of solution, *Chem. Engng Sci.* **27,** 2300–2304, (1972).
16. S. V. Patankar, *Numerical Heat Transfer and Fluid Flow*. McGraw-Hill, New York (1980).
17. S. A. Argyropoulos, Dissolution of high melting point additions in liquid steel, Ph.D. Thesis, Department of Mining and Metallurgical Engineering, McGill University, Canada (1981).
18. P. G. Sismanis, The dissolution of niobium and zirconium in liquid steel, Ph.D. Thesis, Department of Mining and Metallurgical Engineering, McGill University, Canada (1987).
19. G. Kipouros, Private communication, Technical University of Nova Scotia, Halifax, Nova Scotia, Canada (September 1994).
20. *Lange's Handbook of Chemistry* (13th Edn). McGraw-Hill, New York (1985).
21. *Perry's Chemical Engineers' Handbook*. McGraw-Hill, New York (1984).
22. Y. Cao, A. Faghri and W. Chang, A numerical analysis of Stefan problems for generalized multi-dimensional phase-change structures using the enthalpy transforming model, *Int. J. Heat Mass Transfer* **32,** 1289–1298 (1989).
23. K. H. Tacke, Discretization of the explicit enthalpy method for planar phase change, *Int. J. Numer. Meth. Engng* **21,** 543–554 (1985).

APPENDIX 1: RELATIONS OF THERMOPHYSICAL PROPERTIES USED FOR THE COMPUTATIONS

Sulfuric acid solution

Viscosity [Pa s^{-1}]:

$$\mu = 0.000905 + 0.002117 \times C_A - 0.001167 \times C_A^2 + 0.014762 \times C_A^3.$$

Heat capacity [J kg^{-1} K^{-1}]:

$$C_l = 4184.09 - 408.88 \times C_A - 65553.40 \times C_A^2 + 501949.00 \times C_A^3 - 18271170.00 \times C_A^4 + 346600.00 \times C_A^5 - 3599790.00 \times C_A^6.$$

Thermal conductivity [W m^{-1} K^{-1}]:

$$k_l = -0.26826 \times C_A + 0.599267.$$

Density [kg m^{-3}]:

$$\rho = 974.214 + 919.987 \times C_A - 0.75815 \times T.$$

Exothermic heat (partial enthalpy of water [J kg^{-1}]):

$$\Delta\bar{H}_w = 752868 \times C_A^4 + 2011350 \times C_A^3 - 1147570 \times C_A^2 + 252789 \times C_A - 4160.68.$$

Thermal coefficient of volume expansion [K^{-1}]:

$$\beta_T = 0.0001938 \times C_A + 0.000371.$$

Concentration coefficient of volume expansion:

$$\beta_C = -0.249717 \times C_A + 0.711659.$$